

See discussions, stats, and author profiles for this publication at: <https://www.researchgate.net/publication/271332595>

# Catalytic Transformation of Aliphatic Alcohols to Corresponding Esters in O<sub>2</sub> under Neutral Conditions Using Visible-Light Irradiation

ARTICLE in JOURNAL OF THE AMERICAN CHEMICAL SOCIETY · JANUARY 2015

Impact Factor: 12.11 · DOI: 10.1021/ja511619c · Source: PubMed

---

CITATIONS

2

---

READS

71

## 8 AUTHORS, INCLUDING:



Qi Xiao

Queensland University of Technology

14 PUBLICATIONS 144 CITATIONS

[SEE PROFILE](#)



Sarina Sarina

Queensland University of Technology

21 PUBLICATIONS 522 CITATIONS

[SEE PROFILE](#)



James D Riches

Queensland University of Technology

42 PUBLICATIONS 1,336 CITATIONS

[SEE PROFILE](#)



H. Y. Zhu

Queensland University of Technology

189 PUBLICATIONS 7,251 CITATIONS

[SEE PROFILE](#)

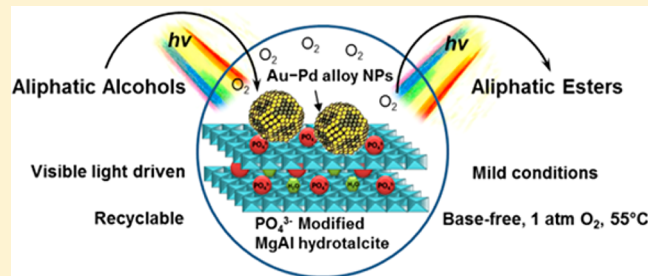
# Catalytic Transformation of Aliphatic Alcohols to Corresponding Esters in O<sub>2</sub> under Neutral Conditions Using Visible-Light Irradiation

Qi Xiao,<sup>†</sup> Zhe Liu,<sup>†</sup> Aixin Bo,<sup>†</sup> Sifani Zavahir,<sup>†</sup> Sarina Sarina,<sup>†</sup> Steven Bottle,<sup>†</sup> James D. Riches,<sup>‡,§</sup> and Huaiyong Zhu\*,<sup>†</sup>

<sup>†</sup>School of Chemistry, Physics and Mechanical Engineering, Science and Engineering Faculty, <sup>‡</sup>Institute for Future Environments, and <sup>§</sup>School of Earth, Environmental and Biological Sciences, Queensland University of Technology, Brisbane, QLD 4001, Australia

## Supporting Information

**ABSTRACT:** Selective oxidation of aliphatic alcohols under mild and base-free conditions is a challenging process for organic synthesis. Herein, we report a one-pot process for the direct oxidative esterification of aliphatic alcohols that is significantly enhanced by visible-light irradiation at ambient temperatures. The new methodology uses heterogeneous photocatalysts of gold–palladium alloy nanoparticles on a phosphate-modified hydrotalcite support and molecular oxygen as a benign oxidant. The alloy photocatalysts can absorb incident light, and the light-excited metal electrons on the surface of metal nanoparticles can activate the adsorbed reactant molecules. Tuning the light intensity and wavelength of the irradiation can remarkably change the reaction activity. Shorter wavelength light (<550 nm) drives the reaction more efficiently than light of longer wavelength (e.g., 620 nm), especially at low temperatures. The phosphate-exchanged hydrotalcite support provides sufficient basicity (and buffer) for the catalytic reactions; thus, the addition of base is not required. The photocatalysts are efficient and readily recyclable. The findings reveal the first example of using “green” oxidants and light energy to drive direct oxidative esterification of aliphatic alcohols under base-free, mild conditions.



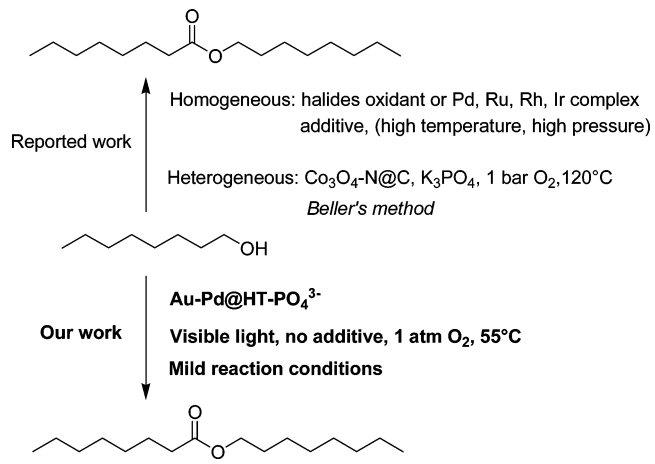
Visible light driven  
Recyclable  
Mild conditions  
Base-free, 1 atm O<sub>2</sub>, 55°C

## 1. INTRODUCTION

Esterification is one of the most essential reactions in organic synthesis.<sup>1–3</sup> Traditionally, esters are prepared by the reaction of activated acid derivatives with alcohols,<sup>4</sup> a multistep process that often produces large amounts of unwanted byproducts. Typically, alcohols are readily available as bulk chemicals and so represent attractive starting materials for large-scale production. In this regard, the direct conversion of alcohols into esters represents a significant advance toward green, economic, and sustainable processes.<sup>5–9</sup> One such process involves the selective oxidation of aliphatic alcohols to the corresponding carbonyl compounds. Among the possible alcohol oxidation reactions, the catalytic and selective oxidation of aliphatic alcohols with molecular oxygen is rather challenging, especially at neutral pH and when employing only moderate reaction conditions.<sup>10</sup> To date, only a very few examples are known for the direct self-esterification of aliphatic alcohols. Of these studies, most involve homogeneous catalytic systems (Scheme 1), such as those using iodide or bromide as oxidant,<sup>11–14</sup> or transition-metal-complex catalysts (Pd, Ru, Rh, Ir, etc.).<sup>15–23</sup> Furthermore, a mild base must be added to counter the acid generated in the process.<sup>11–23</sup> More significantly, most homogeneous catalysis requires harsh reaction conditions, such as high temperatures and high pressures.<sup>15–23</sup>

Therefore, the development of an environmentally benign heterogeneous catalyst for the esterification of aliphatic alcohols

**Scheme 1. Direct Oxidative Esterification of Aliphatic Alcohol (1-octanol as example)**



continues to attract significant interest. For example, Beller and co-workers demonstrated that easily reusable Co<sub>3</sub>O<sub>4</sub>–N@C catalysts can efficiently drive the direct oxidative esterification of aliphatic alcohols.<sup>24</sup> While efficient, this reaction needs to be

Received: November 18, 2014

conducted under 1 bar of O<sub>2</sub> and 120 °C (Scheme 1).<sup>24</sup> Powell and Stahl reported a heterogeneous catalyst consisting of Pd/charcoal in combination with bismuth(III) nitrate and tellurium metal that efficiently esterifies aliphatic alcohols.<sup>25</sup> This process could be achieved under much milder conditions (1 atm of O<sub>2</sub>, 50 °C) compared with Beller's method, but a strong base, potassium methoxide, was used, and the mixed solid catalysts were not easily recycled after the reaction. Overall, the use of heterogeneous catalysts for the direct oxidative esterification of aliphatic alcohols is rarely reported.

Herein we describe a visible-light-driven, one-pot process for direct oxidative esterification of aliphatic alcohols that uses molecular oxygen as oxidant and exhibits high product selectivity under mild conditions. Gold–palladium alloy nanoparticles (Au–Pd alloy NPs) are used as a recyclable photocatalyst for the esterification of aliphatic alcohols, which proceeds under irradiation without the addition of base (Scheme 1).

The discovery of this novel catalytic process derives from our recent development of novel Au–Pd alloy NP photocatalyzed aryl alcohol oxidations using visible light.<sup>26</sup> While investigating the selective oxidation of benzyl alcohol, we observed the trace formation of esters as side products. Addition of a base to remove acid was seen to increase the ester yield. We envisioned that Au–Pd alloy NPs could be useful for the direct self-esterification of aliphatic alcohols, driven by visible-light irradiation. This challenging goal would be of clear significance and broad interest, especially if the addition of base could be avoided. In this regard, an integrated photocatalyst design that relies on the synergy of the metal NPs and support material should in principle be particularly effective toward this goal. On the basis of the fact that K<sub>3</sub>PO<sub>4</sub> or K<sub>2</sub>CO<sub>3</sub> has been used as an additive to enhance the catalyst performance,<sup>12,13,16,18,20,24</sup> we theorized that the addition of base may not be required if basic sites are present as part of the NP-supporting material. By combining the Au–Pd alloy NPs with such supports we could thereby provide a new heterogeneous photocatalyst for base-free oxidation reactions.

In the present study, we have used ion exchange to introduce phosphate anions into hydrotalcite (with a formula of [Mg<sub>6</sub>Al<sub>2</sub>(OH)<sub>16</sub>]CO<sub>3</sub>·mH<sub>2</sub>O and abbreviated HT) to obtain a unique acid-buffering support material (HT-PO<sub>4</sub><sup>3-</sup>) and then loaded Au–Pd alloy NPs onto the HT-PO<sub>4</sub><sup>3-</sup> support material. This unique structure can effectively couple the basic sites of the support material with the photocatalytic properties of the alloy NPs, for the direct self-esterification of aliphatic alcohols under irradiation. Thus, the direct esterification of aliphatic alcohols can be driven without any additive under visible-light irradiation and benign reaction conditions. Notably, these heterogeneous catalysts can be easily recycled and conveniently reused, which has been regarded as an important aspect in the development of practical and cost-effective catalytic oxidation processes. The results reveal a potential route toward greener commercial process for clean and efficient production of aliphatic esters.

## 2. EXPERIMENTAL SECTION

**2.1. Preparation of Catalysts. Mg–Al HT.** The Mg–Al HT with a Mg/Al ratio of 3 was produced using a sol–gel process following established procedures with some modification.<sup>27,28</sup> First, Mg(NO<sub>3</sub>)<sub>2</sub>·6H<sub>2</sub>O (115.4 g, 0.45 mol) and Al(NO<sub>3</sub>)<sub>3</sub>·9H<sub>2</sub>O (56.3 g, 0.15 mol) were dissolved in 0.6 L of deionized water to form an acidic aqueous solution. Then NaOH (60.0 g, 1.5 mol) and Na<sub>2</sub>CO<sub>3</sub> (26.5 g, 0.25

mol) were dissolved in 1.0 L of deionized water to form another alkaline solution. Both of these two solutions were heated to 75 °C. For the preparation of HT, the acidic and alkaline solutions were added dropwise simultaneously into 400 mL of deionized water at 75 °C to obtain the precipitation. The pH value was measured to be 10. The suspension was aged for 3 h at 85 °C under vigorous stirring. After being cooled down to room temperature, the gel suspension was filtered and transferred into an autoclave that was subsequently kept at 80 °C for 16 h. The hydrothermally treated gel was washed with deionized water (350 mL) until the washings reached a pH of 7. The resultant white precipitate was dried in an oven overnight at 80 °C and ground to a powder.

The HT was calcined to 450 °C (heating rate 10 °C·min<sup>-1</sup>) in a flow of 100 mL·min<sup>-1</sup> of dry air for 8 h in preparation, yielding mixed oxides of magnesium and aluminum, which were used for the subsequent ion exchange process.

**Phosphate-Modified HT (HT-PO<sub>4</sub><sup>3-</sup>).** The calcined HT (2.0 g) was dispersed into 50 mL of Na<sub>3</sub>PO<sub>4</sub> aqueous solution (0.02 mmol/L), the suspension was stirred at room temperature for 12 h, the solid was washed and dried at 110 °C for 10 h, and the resultant solid was ground and denoted as HT-PO<sub>4</sub><sup>3-</sup>.

**Au–Pd@HT-PO<sub>4</sub><sup>3-</sup> Catalyst.** Au–Pd@HT-PO<sub>4</sub><sup>3-</sup> catalyst was prepared by an impregnation–reduction method. A 2.0 g portion of HT-PO<sub>4</sub><sup>3-</sup> powder was placed in a 100 mL beaker, and HAuCl<sub>4</sub> (15.2 mL, 0.01 M) and PdCl<sub>2</sub> (28.3 mL, 0.01 M) aqueous solutions were added into the beaker under magnetic stirring at room temperature. Meanwhile, lysine (16 mL, 0.53 M) aqueous solution was added, and the suspension was kept stirring vigorously for 30 min. The pH value of the suspension was measured to be 8–9. Then, a freshly prepared NaBH<sub>4</sub> (3 mL, 0.35 M) aqueous solution was added dropwise over 20 min. After standing for 24 h, the solid was separated by centrifugation (3000 rpm), washed with deionized water (three times) and ethanol (once), and finally dried at 60 °C in a vacuum oven for 24 h. The dried sample can be used as the photocatalyst directly. Monometallic Au/Pd catalysts were prepared in a similar method using HAuCl<sub>4</sub> and PdCl<sub>2</sub> aqueous solutions, respectively.

**2.2. Characterization of Catalysts.** The particle size and morphology of the catalyst samples were characterized with a JEOL2100 transmission electron microscope (TEM), equipped with a Gatan Orius SC1000 CCD camera. Scanning electron microscope (SEM) imaging, elemental mapping, and EDS were performed using a ZEISS Sigma SEM at accelerating voltages of 20 kV. X-ray diffraction (XRD) patterns of the samples were recorded on a Philips PANalytical X'Pert PRO diffractometer using Cu K $\alpha$  radiation ( $\lambda = 1.5418 \text{ \AA}$ ) at 40 kV and 40 mA. The diffraction data were collected from 5° to 75° with a resolution of 0.01° (2θ). Nitrogen physisorption isotherms were measured at -196 °C on a Tristar II 3020. Prior to each measurement, the sample was degassed at 150 °C for 16 h under high vacuum. The specific surface area was calculated by the Brauner–Emmet–Teller (BET) method from the data in a P/P<sup>0</sup> range between 0.05 and 0.2. Temperature-programmed desorption of ammonia (NH<sub>3</sub>-TPD) was conducted on a Micromeritics AutoChem II 2920 chemisorption analyzer to determine the acidic properties of the catalysts. Catalyst samples were activated at 450 °C for 1 h in a vacuum. Ammonia was adsorbed at 1 mbar and 100 °C for 1 h. For desorption, the samples were heated to the corresponding temperature from 100 to 600 °C at a rate of 10 K·min<sup>-1</sup>; desorbing gases were monitored with a Pfeiffer mass spectrometer. A Varian Cary 5000 spectrometer (with BaSO<sub>4</sub> as the reference) was used to collect the data for the diffuse reflectance UV–visible (DR–UV–vis) spectra of the samples.

**2.3. Photocatalytic Reactions.** The photocatalytic reaction was conducted in a light-reaction chamber. A 20 mL Pyrex glass tube ( $\varphi$ , 12 mm) was used as the reaction container. After adding the reactants and catalyst, the tube was filled with O<sub>2</sub> and sealed with a rubber septum cap. Then the tube was stirred with a magnetic stirrer and irradiated under a halogen lamp (Nelson Industries, 500 W tungsten linear halogen lamp, with wavelength in the range 400–750 nm; the light intensity was measured to be 0.5 W/cm<sup>2</sup>). In order to control the reaction temperature carefully, an air conditioner was set and attached to the light-reaction chamber. The reaction temperature under

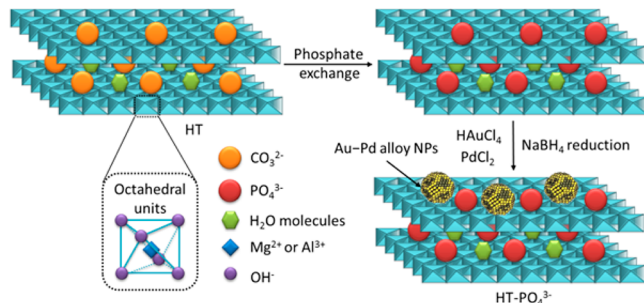
irradiation was maintained the same as the reaction in the dark to make sure that the comparison is meaningful. All the reactions in the dark were conducted using a water bath placed on a magnetic stirrer. In order to strictly avoid exposure of the reaction to light, the tube was wrapped with aluminum foil. After the reaction, 0.5 mL aliquots were collected and then filtered through a Millipore filter (pore size 0.45  $\mu\text{m}$ ) to remove the solid photocatalyst particulates. The products were analyzed by an Agilent 6890 gas chromatography (GC) with HP-5 column. An Agilent HP5973 mass spectrometer was used to identify the product.

Action spectrum experiments were conducted with light emission diode (LED) lamps (Tongyifang, Shenzhen, China) with wavelengths  $360 \pm 5$ ,  $400 \pm 5$ ,  $470 \pm 5$ ,  $530 \pm 5$ ,  $590 \pm 5$ , and  $620 \pm 5$  nm used as the light source. The environmental temperature was measured to be  $45 \pm 2$  °C, and all the other reaction conditions were kept identical with the typical procedures. The apparent quantum efficiency (AQE) was calculated as  $\text{AQE} = [(N_{\text{light}} - N_{\text{dark}})/(\text{the number of incident photons})] \times 100\%$ , where  $N_{\text{light}}$  and  $N_{\text{dark}}$  are the number of products formed under irradiation and in the dark, respectively.

### 3. RESULTS AND DISCUSSION

**3.1. Catalyst Synthesis and Characterization.** HT solids are known to possess surface basic properties that can be fine-tuned by their compositions.<sup>29–31</sup> In this study, the phosphate-modified HT support (HT-PO<sub>4</sub><sup>3–</sup>) was prepared by utilizing the “memory effect” of HT. The HT solid was calcined to 450 °C, yielding mixed oxides of magnesium and aluminum. When the mixed oxide powder was dispersed into Na<sub>3</sub>PO<sub>4</sub> aqueous solution, the layered double hydroxide structure was restored, but the anions between the layers are phosphate anions. The resultant solid was used as a support for Au–Pd alloy catalysts (Scheme 2).

**Scheme 2. Preparation of Au–Pd@HT-PO<sub>4</sub><sup>3–</sup> Catalysts**



As shown in the representative TEM images of the catalysts (Figure 1), the alloy NPs are distributed evenly on the HT surface (Figure 1a), and the average diameter of the NPs is approximately 4–5 nm (Figure 1b). The high-resolution TEM (HR-TEM) images reveal the atom lattices of Au–Pd alloy NPs (Figure 1c,d). The lattice fringe spacing of 0.23 nm corresponds to the interplanar distance of (111) planes in the Au–Pd alloy lattice (Figure 1d).

To investigate the elemental composition in the as-prepared photocatalyst, energy-dispersive X-ray spectroscopy (EDX) elemental mappings of the Au–Pd@HT-PO<sub>4</sub><sup>3–</sup> catalyst were performed (Figure 2a). EDX elemental mapping of the SEM image shows that all the components are homogeneously distributed throughout the sample. The phosphorus element is clearly evidenced in the mapping data, and the phosphorus signals indicate that the doped phosphate anion is uniformly distributed in the HT sample. The percentages of Mg, Al, P, Au, and Pd elements in the catalysts were also analyzed from

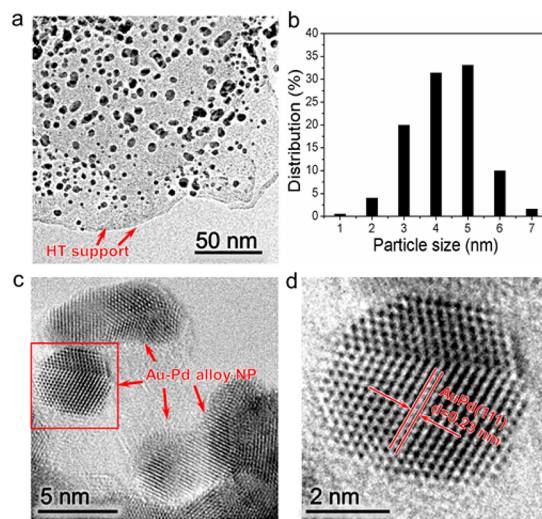


**Figure 1.** (a) TEM image of the samples. (b) Particle size distribution of the NPs based on the statistical analysis of TEM images (by measuring >350 isolate particles in the images of the sample). (c) HR-TEM image of the alloy NPs. (d) HR-TEM image of an alloy particle indicated in part c (red square).

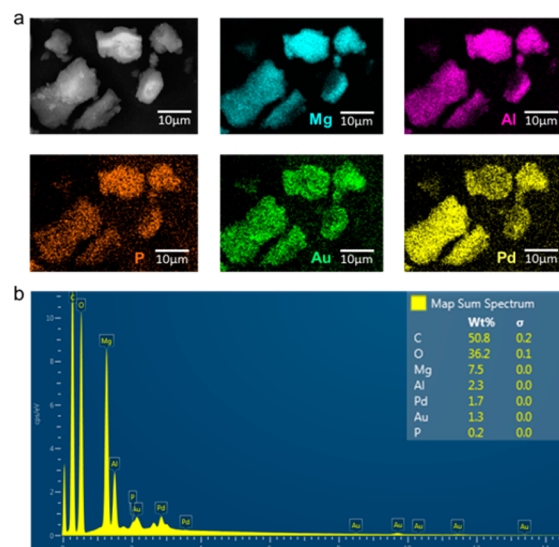


**Figure 2.** (a) Scanning electron microscopy (SEM) image of a typical Au–Pd@HT-PO<sub>4</sub><sup>3–</sup> sample and the corresponding energy dispersive spectrometer (EDX) mapping of Mg, Al, P, Au, and Pd elements. (b) EDX spectrum.

the EDX spectrum (Figure 2b); the Mg/Al ratio (3/1) and Au/Pd ratio (1/1) are matched with the initial experimental design.

The well-defined, layered structure characteristic of HT is confirmed for all samples by the X-ray diffraction (XRD) patterns (Figure 3). It is clear that all diffraction peaks could be indexed to the HT structure, and the structure was restored after introducing phosphate anions and remained unchanged after the metal NPs were loaded, although the intensity of the diffraction peaks decreased and their widths increased. No reflections assignable to Au and Pd are present in the XRD patterns, possibly because the low metal content was below the detection limit and/or due to poor crystallinity of the metal NPs on the surface of HT.

The light-absorption properties of the samples can also confirm the formation of Au–Pd alloy NPs. As shown in Figure

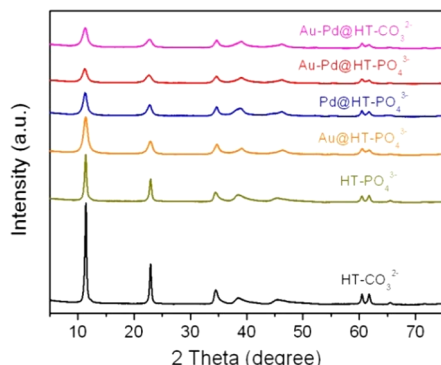


**Figure 3.** XRD patterns of the photocatalysts.

4, the  $\text{HT-PO}_4^{3-}$  support exhibits weak absorption in the range of visible-light wavelengths above 400 nm, and therefore, the

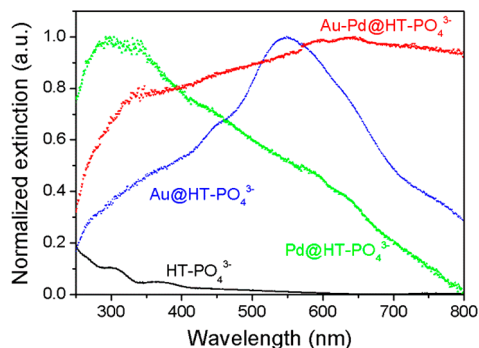


**Figure 4.** Normalized diffuse reflectance ultraviolet–visible (DR-UV/vis) extinction spectra of the photocatalysts.

support itself cannot contribute to the photocatalytic activity. In contrast, all the NP photocatalysts display strong absorption in the UV and visible ranges of the spectrum, indicating that the NPs are able to utilize most of the irradiation energy delivered

in the solar spectrum. The presence of the support and its interaction with the NPs can substantially shift and broaden the light-absorption peaks.<sup>32</sup> The spectrum of the Au–Pd alloy NPs sample is apparently different from the spectra of metal NPs of either pure component. The dielectric constant of the alloy NPs is different from the pure metal NPs, and the light absorption of the metal NPs depends substantially on their dielectric constant. In the spectrum of the alloy sample, the characteristic localized surface plasmon resonance (LSPR) absorption peak of Au NPs at about 520 nm is weaker compared with the spectrum of a pure Au sample. The main absorption peak of the pure Pd NPs on the support is at about 300 nm in the UV region, and its light absorption at solar wavelengths occurs through the light excitation of the electron to higher energy levels.<sup>33</sup> Obviously, the absorption of the alloy NPs in the visible range is more intense than that observed for pure Pd sample. This means that the alloy NPs have a better ability to gain light energy to enhance their catalytic performance when irradiated with visible light.

**3.2. Photocatalytic Performance.** Exploratory photocatalytic experiments with the different catalytic materials were performed using the oxidative esterification of 1-octanol to give octyl octanoate as a model reaction. For comparison, the dark reactions were conducted without irradiation and all the other reaction conditions were kept identical. Typically, the reaction temperature in the dark was maintained the same as the reaction under irradiation by using a water bath.

To understand the effect of various bases on the performance of the catalytic system, we used Au–Pd@ $\text{ZrO}_2$  catalysts with various base additives [Table S1, Supporting Information (SI)] and found that when using  $\text{K}_3\text{PO}_4$  as the base the photocatalytic reaction exhibited the best performance, and this is in agreement with the literature report that  $\text{K}_3\text{PO}_4$  is the optimal base additive for the oxidative esterification.<sup>20,24</sup> The performance of the alloy NPs on the unmodified HT was also examined. As can be seen in Table 1, Au–Pd@HT catalyst exhibits a slightly better performance under visible-light irradiation (entry 1) than in the dark for the direct oxidative

**Table 1. Activity Test and Catalyst Screening for Oxidative Esterification of 1-Octanol<sup>a</sup>**

entry	catalyst	additive	incident light		
				conversion (%)	selectivity (%)
1	Au–Pd@HT	—	visible	48	54
		—	dark	45	3
2	Au–Pd@HT	$\text{K}_3\text{PO}_4$	visible	78	62
		$\text{K}_3\text{PO}_4$	dark	57	25
3	Au–Pd@HT- $\text{PO}_4^{3-}$	—	visible	94	76
		—	dark	62	42
4	Au@HT- $\text{PO}_4^{3-}$	—	visible	35	72
		—	dark	24	68
5	Pd@HT- $\text{PO}_4^{3-}$	—	visible	84	58
		—	dark	60	31
6	Au@HT- $\text{PO}_4^{3-}$ + Pd@HT- $\text{PO}_4^{3-}$	—	visible	54	63
		—	dark	46	34
7	$\text{HT-PO}_4^{3-}$	—	visible	0	0
		—	dark	0	0

<sup>a</sup>Reaction conditions: photocatalyst, 100 mg; reactant, 0.2 mmol; additive, 50 mg; solvent, 2 mL of  $\alpha,\alpha,\alpha$ -trifluorotoluene; 1 atm of  $\text{O}_2$ ; environment temperature, 55 °C; reaction time, 24 h; and light intensity, 0.5 W/cm<sup>2</sup>. The conversions and selectivity were calculated from the product formed and the reactant converted, as measured by gas chromatography (GC).

esterification of 1-octanol. Adding  $K_3PO_4$  increases the reaction activity of this catalyst (entry 2). To our delight, the alloy NPs on the  $PO_4^{3-}$ -modified HT, Au–Pd@HT- $PO_4^{3-}$  catalyst, exhibit optimal performance for the one-pot oxidative esterification. Excellent conversion (94%) and good selectivity (76%) were achieved without any additional base additive under visible-light irradiation (entry 3). A much lower activity was observed for the reaction in the dark (entry 3). Several commonly used solvents were examined for the reaction, while other reaction conditions were maintained unchanged (Table S2, SI), and it was found that  $\alpha,\alpha,\alpha$ -trifluorotoluene exhibited the best performance. The catalytic activities of the monometallic Au and Pd catalyst as well as a mixture of monometallic Au and Pd catalysts (entry 4–6) are obviously lower than that of the alloy NP catalyst. Interestingly, Pd@HT- $PO_4^{3-}$  is a superior catalyst to Au@HT- $PO_4^{3-}$  both under the visible-light irradiation and in the dark. This could be attributed to the better ability of Pd NPs to activate molecular oxygen<sup>34–36</sup> and the fact that irradiation can enhance the catalytic performance of Pd NPs.<sup>33</sup>

These results indicate that the alloying of the two metals can further enhance the catalytic activity, which is in line with our previous reported results.<sup>26</sup> The alloy NP surface has greater charge heterogeneity than pure metal NP surface, which can result in a stronger interaction between the surface of NPs and the adsorbed reactant molecules, facilitating the reaction. Compared with recently reported heterogeneous catalysts for the direct oxidative esterification of 1-octanol at 120 °C under 1 bar of  $O_2$ , which achieved a octyl octanoate yield of 75%,<sup>24</sup> the Au–Pd alloy NP photocatalyst in the present study is efficient and much more environmentally friendly. We also conducted the reactions with Au–Pd@HT- $PO_4^{3-}$  catalyst under simulated sunlight irradiation: under an irradiance (light intensity) of 0.45 W/cm<sup>2</sup> (55 °C), 82% conversion was obtained, with 80% octyl octanoate selectivity, which is much higher than that of the control experiment in the dark (Table S3, SI). To the best of our knowledge, the metal NPs or Au–Pd alloy NPs on HT-based materials have not been found to be efficient base-free oxidation catalysts under mild conditions. The present study is also the first successful example of the direct oxidative esterification of aliphatic alcohols under base-free conditions with visible light. Notably, the novel catalyst system is highly stable and can be reused several times (see below).

The direct oxidative esterification of a series of aliphatic alcohols catalyzed by the Au–Pd@HT- $PO_4^{3-}$  catalyst was also investigated. As shown in Table 2, good yields of the corresponding aliphatic esters were achieved. Notably, the product yields for the reactions under irradiation are much higher than those of typical thermal reactions undertaken in the dark.

The successful self-esterification of aliphatic alcohols also inspired us to explore the selective oxidative cross-couplings of aryl alcohols with alkyl alcohols to yield different alkyl esters. Such selective cross-esterification reactions have been scarcely studied in the past due to the potential problem of oxidizing one alcohol in the presence of another.<sup>24</sup> Moreover, most of the reported selective cross-esterifications require high reaction temperature and high oxygen pressure.<sup>18,24,37</sup> In the present study, the oxidative cross-esterifications of benzyl alcohol with methanol and ethanol as well as 1-octanol were investigated, which yield corresponding aryl esters in different solvents. By using Au–Pd@HT- $PO_4^{3-}$  catalyst under visible-light irradiation, yields up to 76% were achieved (Table 3, entries 1–4).

**Table 2. Photocatalytic Base-Free Direct Oxidative Esterification of Various Aliphatic Alcohols<sup>a</sup>**

R=aliphatic	$R-\text{CH}_2-\text{OH} \xrightarrow[\text{1 atm } O_2, 55^\circ\text{C, 24 h}]{\text{Au-Pd@HT-}PO_4^{3-}, h\nu}$	ester
1		73 (40)
2		75 (44)
3		72 (26)
4		47 (13)
5		53 (12)

<sup>a</sup>Reaction conditions: Au–Pd@HT- $PO_4^{3-}$  photocatalyst, 100 mg; reactant, 0.2 mmol; solvent, 2 mL of  $\alpha,\alpha,\alpha$ -trifluorotoluene; 1 atm of  $O_2$ ; environment temperature, 55 °C; reaction time, 24 h; and light intensity, 0.5 W/cm<sup>2</sup>. <sup>b</sup>The yields were calculated from the product formed and the reactant converted, as measured by GC; the values in parentheses are the results in the dark.

**Table 3. Photocatalytic Base-Free Selective Oxidative Cross Couplings of Aryl Alcohols with Alkyl Alcohols<sup>a</sup>**

Entry	Reactant	Product	Yield (%) <sup>b</sup>
1 <sup>c</sup>			76 (50)
2 <sup>c</sup>			40 (16)
3 <sup>d</sup>			51 (23)
4 <sup>e</sup>			30 (3)
5 <sup>f</sup>			43 (17)

<sup>a</sup>Reaction conditions: Au–Pd@HT- $PO_4^{3-}$  photocatalyst, 50 mg; reactant, 0.2 mmol; 2 mL of solvent; 1 atm of  $O_2$ ; environment temperature, 55 °C; reaction time, 24 h; light intensity, 0.5 W/cm<sup>2</sup>.

<sup>b</sup>The yields were calculated from the product formed and the reactant converted, as measured by GC; the values in parentheses are the results in the dark. <sup>c</sup>Methanol as solvent. <sup>d</sup>Ethanol as solvent. <sup>e</sup>1-Octanol as solvent. <sup>f</sup>n-Heptane as solvent.

However, when the methoxy group was situated in the ortho position, the ester yield declined to 40% (Table 3, entry 2), which may due to the stereohindrance effect of the substituent. Here, the esterification with aliphatic 1-octanol is known to be much more challengeable, yet we can still achieve a decent yield of 30% using visible-light irradiation (Table 3, entry 4). Finally, we also performed the self-esterification of benzyl alcohol (Table 3, entry 5); again, the catalyst exhibited high activity and selectivity under visible-light irradiation, achieving a 43% yield of the corresponding benzyl benzoate.

The Au–Pd@HT- $PO_4^{3-}$  photocatalysts are also effective for the oxidation of secondary aliphatic alcohols to ketones.

Excellent aliphatic ketone yields were achieved under base-free, mild reaction conditions (Table 4).

**Table 4. Photocatalytic Base-Free Oxidation of Secondary Aliphatic Alcohols to Ketones<sup>a</sup>**

Entry	Reactant	Product	Yield (%) <sup>b</sup>	Au-Pd@HT-PO <sub>4</sub> <sup>3-</sup> , hν	
				1 atm O <sub>2</sub> , 55 °C, 24 h	R=alkyl
1			100 (19)		
2			91 (17)		

<sup>a</sup>Reaction conditions: Au-Pd@HT-PO<sub>4</sub><sup>3-</sup> photocatalyst, 50 mg; reactant, 0.2 mmol; solvent, 2 mL of *α,α,α*-trifluorotoluene; 1 atm of O<sub>2</sub>; environment temperature, 55 °C; reaction time, 24 h; and light intensity, 0.5 W/cm<sup>2</sup>. <sup>b</sup>The yields were calculated from the product formed and the reactant converted, as measured by GC; the values in parentheses are the results in the dark.

A key attraction to heterogeneous catalysis is the possibility of catalyst recycling. We carried out a series of experiments using oxidative esterification of 1-octanol under irradiation to demonstrate the recyclability of Au-Pd@HT-PO<sub>4</sub><sup>3-</sup> catalyst. Briefly, after each reaction cycle, Au-Pd@HT-PO<sub>4</sub><sup>3-</sup> catalyst was separated by centrifugation, washed thoroughly by ethanol twice, and dried for subsequent reactions. As shown in Figure 5a, the catalyst was reused for several cycles without significant

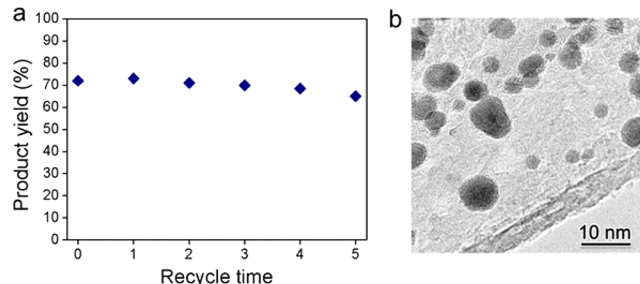


**Figure 5.** (a) The photocatalytic activity of the Au-Pd@HT-PO<sub>4</sub><sup>3-</sup> catalyst after being recycled five times. (b) Representative TEM image of the Au-Pd@HT-PO<sub>4</sub><sup>3-</sup> catalyst after being recycled. The dark particles are the alloy NPs.

loss of activity. From the typical TEM image of the Au-Pd@HT-PO<sub>4</sub><sup>3-</sup> catalyst after being recycled (Figure 5b), the metal NPs still distribute evenly on the surface of HT support, and no obvious agglomeration was observed.

**3.3. Influence of the Supports.** Since the oxidative esterification can proceed in the absence of added base, the surface properties of the support materials of the photocatalysts are expected to play a critical role in catalyst performance. Specific surface areas of the photocatalysts (derived from nitrogen sorption data) and the surface acidity of the samples (measured by NH<sub>3</sub> temperature-programmed desorption, NH<sub>3</sub>-TPD) are provided in Table 5. The specific surface area is not the decisive factor on the performance, as the optimal photocatalyst has a relatively small specific surface area. Basic sites on the support surface alone cannot simply be the dominate factor enhancing the catalyst performance, since MgO and HT have basic surface sites but Au-Pd@MgO and

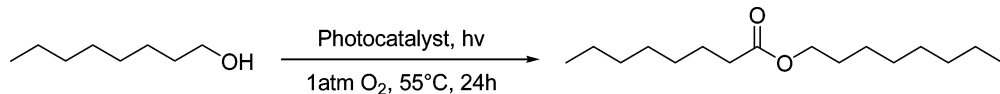
Au-Pd@HT exhibit low and moderate activity, respectively. We also found that the oxidative esterification activity of the Au-Pd@HT-PO<sub>4</sub><sup>3-</sup> catalyst can be greatly inhibited by the addition of benzoic acid or pyridine (Scheme S1, SI). This is likely to arise from interference with the basic/acidic sites of the support by reaction with the benzoic acid or pyridine<sup>31</sup> and potentially by surface complexation of the benzoate or pyridinium conjugate ions limiting access by the alcohol substrate. Therefore, a moderate population of basic/acidic sites on the supports is necessary for the catalysis, and the basic surface sites from PO<sub>4</sub><sup>3-</sup> are superior to other basic sites for the catalytic performance. The unique surface character of the Au-Pd@HT-PO<sub>4</sub><sup>3-</sup> catalyst is essential for facilitating the base-free direct oxidative esterification of aliphatic alcohols. The content of PO<sub>4</sub><sup>3-</sup> in the HT support also affects the catalytic activity (Table S4, SI). According to the results of EDX analysis, when the phosphorus content is 0.2 wt % of the catalyst, the catalyst exhibits the best performance; further increasing the amount of PO<sub>4</sub><sup>3-</sup> can suppress the conversion rate and ester selectivity. Thus, a small amount of phosphate exchanged into the HT support can provide necessary basic/acidic sites for the catalyzed reactions and thus avoid the need to add base for efficient conversion.

#### 3.4. Influence of the Light Intensity and Wavelength.

The relationship between the photocatalytic activity and the incident light intensity (irradiance) was investigated. As depicted in Figure 6, the oxidative esterification of 1-octanol was conducted under different irradiances. When the irradiance was raised, the reaction yields increased. The contributions of irradiation to the conversion efficiency were calculated by subtracting the reaction yield achieved in the dark from the overall yield of the irradiated system when reactions were conducted at identical reaction temperature.<sup>26</sup> The product yield obtained in the dark is regarded as the thermal contribution. The relative contributions of visible-light irradiation to the conversion efficiencies are shown in Figure 6.

The numbers with percentages in Figure 6 show the light irradiation contribution. It can be seen that the higher the irradiance, the greater the contribution of irradiation to the overall reaction rate. When the irradiance is 0.3 W/cm<sup>2</sup>, the light contribution for the reaction is only 46%, and when the irradiance increased to 0.7 W/cm<sup>2</sup>, 74% of the product yield is due to irradiation. A greater irradiance provides more light-excited energetic electrons and creates a stronger electromagnetic field in the vicinity of the NPs (LSPR field enhancement effect).<sup>38–40</sup>

The light-excited metal electrons may facilitate the reaction via two pathways: release energy to the lattice to thereby heat the NPs (photothermal effect) or transfer to the reactant molecules that are adsorbed on the NP, directly causing the reaction of the molecules (excited electron transfer). If the reaction is due to the photothermal effect, the wavelength of the light employed in the irradiation has little impact on the reaction rate when the irradiance is identical. A useful tool for determining whether a reaction is induced due to the photothermal effect is the action spectrum, which shows the relationship between the wavelength of incident light and the photocatalytic rate.<sup>41,42</sup> In the present study, the photocatalytic activity of the oxidative esterification of 1-octanol using Au-Pd@HT-PO<sub>4</sub><sup>3-</sup> catalyst at 45 ± 2 °C under different wavelengths of light irradiation was studied. The obtained reaction yields were used to calculate the apparent quantum efficiencies (AQEs).<sup>33,43</sup> The plot of AQE versus the respective

**Table 5. Activity Test of Different Supports for Base-Free Oxidative Esterification of 1-Octanol<sup>a</sup>**

entry	catalyst	BET surface area ( $\text{m}^2/\text{g}$ ) <sup>b</sup>	acid density (mmol/g) <sup>c</sup>	incident light	conversion (%)	ester selectivity (%)	ester yield (%)
1	Au–Pd@HT-PO <sub>4</sub> <sup>3-</sup>	13	0.91	visible	94	76	72
				dark	62	42	26
2	Au–Pd@HT	59	1.00	visible	48	54	26
				dark	45	3	2
3	Au–Pd@Al <sub>2</sub> O <sub>3</sub>	201	1.07	visible	51	92	47
				dark	33	5	2
4	Au–Pd@MgO	3	0.03	visible	20	34	7
				dark	3	0	0
5	Au–Pd@ZrO <sub>2</sub>	20	0.20	visible	38	47	19
				dark	33	36	12

<sup>a</sup>Reaction conditions: photocatalyst, 100 mg; reactant, 0.2 mmol; solvent, 2 mL of  $\alpha,\alpha,\alpha$ -trifluorotoluene; 1 atm of O<sub>2</sub>; environment temperature; 55 °C; reaction time, 24 h; and light intensity, 0.5 W/cm<sup>2</sup>. The conversions and selectivity were calculated from the product formed and the reactant converted, as measured by GC. <sup>b</sup>Determined by adsorption–desorption of nitrogen. <sup>c</sup>Determined by NH<sub>3</sub>-TPD.

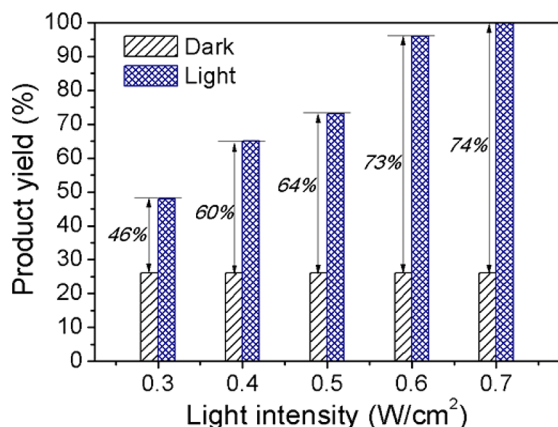


**Figure 6.** Dependence of the catalytic activity of Au–Pd@HT-PO<sub>4</sub><sup>3-</sup> photocatalyst for the oxidative esterification of 1-octanol on the intensity of irradiation. The light contribution =  $[(Y_{\text{light}} - Y_{\text{dark}})/Y_{\text{light}}] \times 100\%$ , where  $Y_{\text{light}}$  and  $Y_{\text{dark}}$  are the product yields under irradiation and controlled in the dark, respectively.

wavelengths is the action spectrum of the reaction. The action spectrum shows that the dependence of the AQE of the reaction catalyzed by the Au–Pd alloy catalysts on the wavelength of irradiation does not track with the light absorption spectrum for the supported Au–Pd@HT-PO<sub>4</sub><sup>3-</sup> catalyst (Figure 7). The highest activity is observed at shorter wavelengths, thus the photothermal effect is not the main pathway for the reaction.

The total input energy absorbed by the photocatalysts under irradiation at different wavelengths was similar for a given reaction period, since the reaction temperature and irradiance were maintained constant at a specific wavelength (Figure 7). The influence from external heating has been excluded from AQE values by deducting the product yield formed in the dark. If a part of the input photon energy is converted into a thermal effect, then the catalytic activity caused by the photothermal effect is similar. The extraordinarily high enhancement in activity with shorter-wavelength photons indicates that photoenhancement at 360 nm is not only due to a simple photothermal effect.<sup>33</sup> It is more likely that the photocatalytic esterification of 1-octanol irradiated with light wavelength

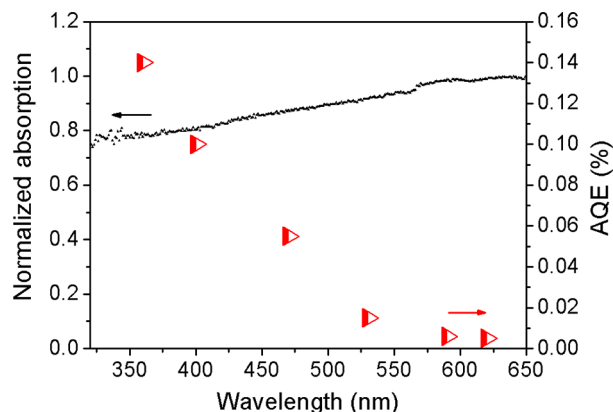


**Figure 7.** Photocatalytic action spectrum for the oxidative esterification of 1-octanol using Au–Pd@HT-PO<sub>4</sub><sup>3-</sup> photocatalyst. The light-absorption spectrum (left axis) is the DR–UV/vis spectra of the supported Au–Pd@HT-PO<sub>4</sub><sup>3-</sup> catalyst (black curve).

shorter than 550 nm mainly proceeds via the excited electron transfer.

The photons with a shorter wavelength are able to excite metal electrons to higher energy levels, and these electrons have more chances to transfer to the antibonding orbitals, located above the bonding orbitals on the energy scale, inducing reaction.<sup>40</sup> When the energy of the antibonding orbital is high, the electrons excited by light with a longer wavelength do not have sufficient energy for the injection. They will relax to low energy levels and release energy to heat the lattice of the alloy NPs, enhancing the reaction only by the photothermal effect. Thus, the photothermal contribution to the AQE obtained under the longest wavelength (620 nm) is the largest, compared to that from the other wavelengths. Therefore, by comparing the AQE observed at short wavelengths with that observed at long wavelengths, we can estimate the contribution from the excited electron transfer.<sup>33</sup> The AQE values at 590 and 620 nm are low, and the AQE values at short wavelengths (<550 nm) are much larger. The large difference between the AQE values at short and long wavelengths means that most of the chemical transformation at short wavelength is via the excited electron transfer pathway. Moreover, the wavelength dependence can also be well-explained by an electron-scattering

process through a high-energy adsorbate affinity state of the reactant molecule with the metal NP surface<sup>44</sup> and a direct photoexcitation process involving high-energy electronic transitions between hybridized metal and adsorbate states.<sup>45</sup> The former suggested that different reactant adsorbates on the metal NP surface will exhibit unique wavelength dependences that are controlled by the strength of their interaction with the primary or nonthermalized energetic electron distribution, and the latter proposed that the strong hybridization and spatial overlap of the reactant adsorbate and metal states that occur due to chemical bond formation may allow direct photoexcitation of metal–adsorbate bonds through dipole electronic transitions involving hybridized metal surface atom–adsorbate states. The impact of nonthermalized electrons on the activation of metal–adsorbate bond results in wavelength dependences that deviate from the light-absorption spectra of the metal NPs. The unique wavelength-dependent photoexcitation of metal NP catalysts may allow us to tune the selectivity of catalytic reactions with irradiation.

We further compared the oxidative esterification of 1-octanol using Au–Pd@HT-PO<sub>4</sub><sup>3-</sup> photocatalyst at various temperatures under 400 and 620 nm LED irradiation, respectively (Figure S3, SI). It can be seen that the catalytic performance of the reaction irradiated with 400 nm wavelength is much better than that irradiated with 620 nm wavelength and in the dark, especially at lower reaction temperature. The dependence of the catalytic activity on the reaction temperature for the reaction irradiated with a long wavelength (620 nm) is very similar to that in the dark.

The dependence of reaction activity on the light irradiance and wavelength suggests that the light-excited electrons play a dominate role in the observed photocatalytic activity.<sup>46</sup> Since the reaction rate is expected to depend on the population of electrons with sufficient energy to induce the reaction of the reactant molecules, one can increase the number of these light-excited “hot” electrons by using higher irradiance or tuning the irradiation wavelength to accelerate the catalytic reaction rate. This knowledge may also help us to better understand the reaction mechanism of the metal NP photocatalysis.<sup>33,38–40,43</sup>

**3.5. Influence of Temperature.** As an important feature of the metal NP photocatalysis, the catalytic activity can be increased by elevating the reaction temperatures.<sup>47,48</sup> This feature is also observed from the Au–Pd alloy NP photocatalysts.<sup>43</sup> In the present study, we conducted the oxidative esterification of 1-octanol using Au–Pd@HT-PO<sub>4</sub><sup>3-</sup> photocatalyst at various temperatures both under irradiation and in the dark.

As shown in Figure 8a, raising the reaction temperature can achieve higher product yields, for both the irradiated reactions and the dark reactions. We calculated the contribution of the irradiation effect as the difference between the yields in the light reaction and the dark reaction divided by the total yield under irradiation. The light contribution =  $\frac{[(Y_{\text{light}} - Y_{\text{dark}})/Y_{\text{light}}]}{\times 100\%}$ , where  $Y_{\text{light}}$  and  $Y_{\text{dark}}$  are the product yields under irradiation and dark conditions, respectively. For example, when at 55 °C, the difference between the light reaction and dark reaction is 47%, accounting for 64% of the total yield. It can be seen that the contribution decreases as the reaction temperature was raised. To further understand the effect of reaction temperature, we compare the action spectra for the photocatalytic reaction at two different temperatures (45 and 70 °C, Figure 8b). Much lower AQEs were obtained at a higher temperature as the increased number of product molecules

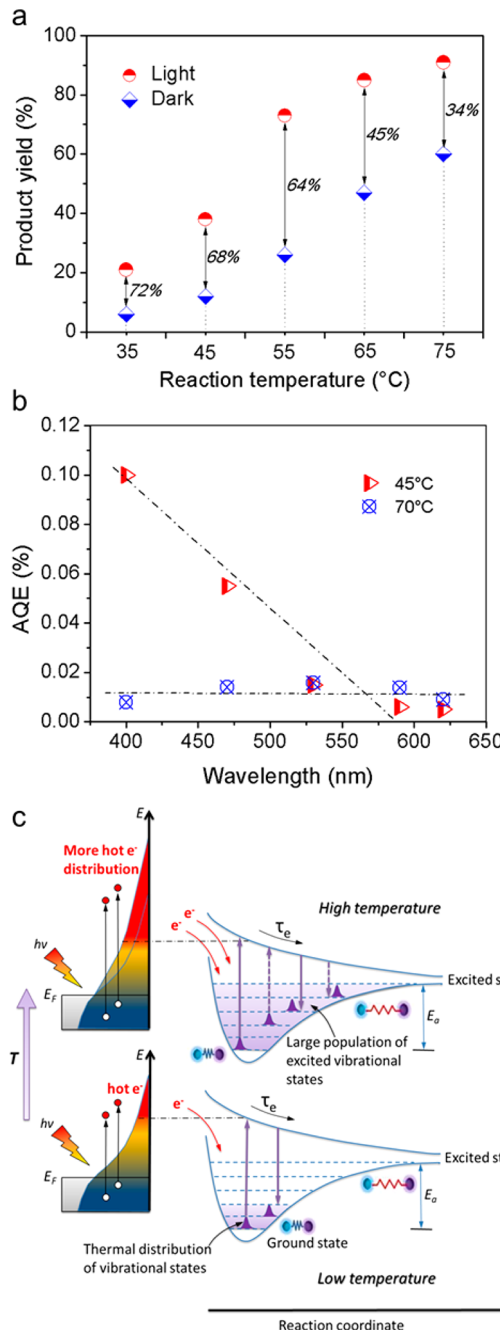


**Figure 8.** (a) The catalytic activities of the oxidative esterification of 1-octanol using Au–Pd@HT-PO<sub>4</sub><sup>3-</sup> photocatalyst at different temperatures under visible-light irradiation and in the dark. The numbers with percentages show the light contribution. (b) Comparison of action spectra for the oxidative esterification of 1-octanol using Au–Pd@HT-PO<sub>4</sub><sup>3-</sup> photocatalyst at two different temperatures. (c) A schematic of the effect of increasing temperature on the gain of vibrational energy, thus facilitating the reaction.

formed in the dark is deducted from the values when the AQE of the irradiated reaction is calculated. The AQE value barely varies with the wavelength of irradiation. As shown in Figure 8c, at a higher temperature, more light-excited electrons can gain sufficient energy for the transfer from metal NP to adsorbed molecules (the longer wavelengths can also excite metal electrons to high energy levels), and the probability of the electron transfer is higher than that of the lower reaction temperature.<sup>46</sup> On the other hand, at higher temperatures, the

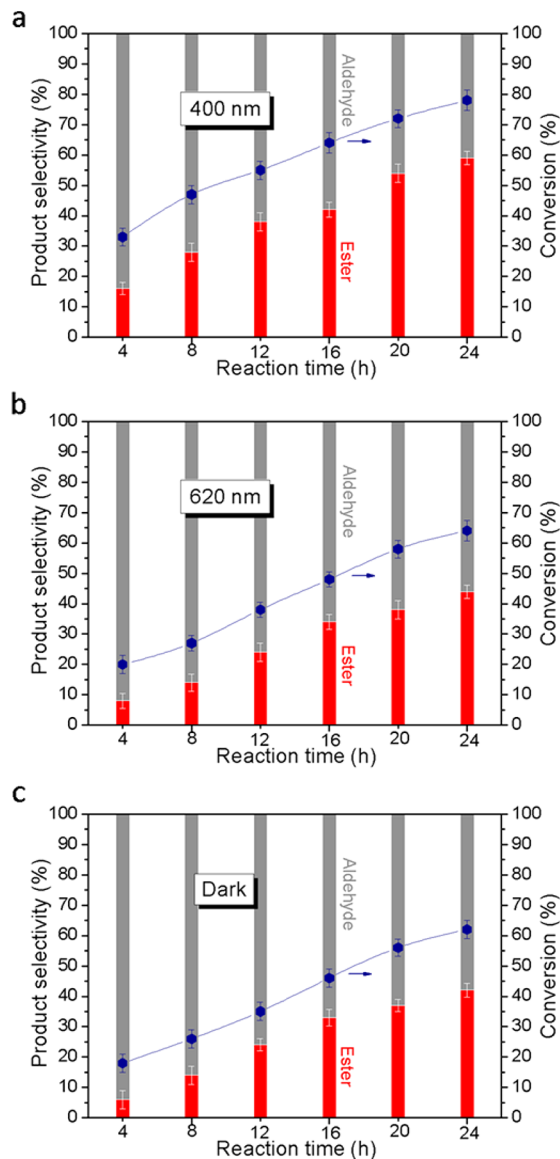
relative population of excited vibrational states of the adsorbed reactant molecules increases according to the Bose–Einstein distribution.<sup>48</sup> This means that, on average, the reactant molecule will require less energy to surmount the activation barrier, and the activation of the alcohol molecule should be much easier. At high temperatures, the contribution from the thermal effect (phonon-driven) can be greater than that from the light irradiation as the reactant molecules may gain most energy from heating to overcome the activation energy barrier. In this case, the thermal energy is sufficient enough to induce a significant population of vibrationally excited states of the reactant molecules,<sup>46,49</sup> while the light-excited electrons can also contribute to accelerating the reactions.<sup>50,51</sup> The light-excited electrons in the high-energy tail of a thermal Fermi–Dirac distribution can induce reactions by a transient population of normally unoccupied states.<sup>50</sup> We can see that light contribution is 72% when the reaction is limited to 35 °C (Figure 8a). At lower temperatures, the excited electron transfer dominates the photocatalytic activity and the thermal effect (and photothermal effect as well) contributes much less.<sup>51</sup> For those reactions in which the interaction of the light-excited electrons of the metal NPs with the adsorbed reactant molecules can induce the reaction, high reaction temperature is not a prerequisite for efficacy.

The above results also demonstrate that the alloy NPs have the capacity to couple the stimuli of irradiation and heat to drive the catalytic reaction due to the continuum of metal electron energy levels.<sup>43,47</sup> This property is apparently different from those of traditional semiconductor photocatalysts, which may show the potential of the NP photocatalysts to utilize the infrared radiation from sunlight to facilitate chemical reactions under ambient conditions.

**3.6. Proposed Reaction Pathway.** To investigate the reaction pathway, we studied the evolution of the products during the time course of the oxidative esterification of 1-octanol using Au–Pd@HT-PO<sub>4</sub><sup>3-</sup> photocatalyst under irradiation with a short-wavelength LED (400 nm) and a long-wavelength LED (620 nm), respectively (parts a and b of Figure 9), and the results are compared with that of the reaction in the dark (Figure 9c).

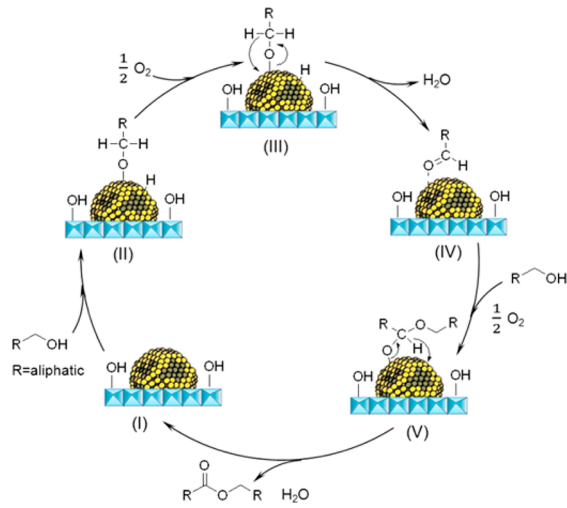
We found that the conversion of the reaction irradiated with a short wavelength is higher than that irradiated with a long wavelength and in the dark. Furthermore, the aldehyde is the main intermediate during the reaction course, both under light irradiation and in the dark. This suggests that the alcohol is first oxidized to aldehyde during the process and then the aldehyde further reacts with another alcohol molecule to achieve the direct esterification.

A tentative mechanism for the direct oxidative esterification of alcohols is proposed on the basis of the literature precedent<sup>13,15,21,24</sup> and is depicted in Scheme 3. The oxidative esterification reaction may proceed through an oxidation of alcohol to aldehyde (IV) and then a condensation reaction between aldehyde and another molecule of alcohol, which results in the formation of a hemiacetal intermediate (V), followed by oxidative dehydrogenation to give the corresponding ester. In this case, the alcohol molecule is adsorbed on the Au–Pd alloy NP surface because the alloy NP surface has a strong binding affinity. The selective oxidation of alcohol to aldehyde on the alloy NP surface is likely to proceed first (I–IV). Irradiation can facilitate the cleavage of the O–H bond for the insertion step, which leads to the formation of metal alkoxide and metal hydride species (II). The surface basic sites



**Figure 9.** Time course for the catalytic activities [reaction conversion and product selectivity (red, ester; gray, aldehyde)] of the oxidative esterification of 1-octanol using Au–Pd@HT-PO<sub>4</sub><sup>3-</sup> photocatalyst under irradiation with 400 nm LED (a), 620 nm LED (b), and in the dark (c) at 55 °C.

of the support can bind the hydrogen atom of the reactant molecule and also facilitate the O–H cleavage on the metal surface, as per reports in the literature.<sup>52</sup> Light-excited electrons can promote hydrogen abstraction from the  $\alpha$ -H of the metal alkoxy species, which then yields the aldehyde (III, IV). DFT calculations also suggest that the transfer of a light-excited electron from metal NP to the reactant molecule adsorbed on the NP surface can facilitate the cleavage of the C–H bond.<sup>26</sup> The presence of surface basic sites also lowers the barrier for the activation of the C–H bond of the metal alkoxide intermediate to form the aldehyde over the metal NP surface.<sup>50</sup> Then the formed aldehyde on the metal NP surface can react with another molecule of alcohol and form the hemiacetal intermediate (V).<sup>13,15,21,24</sup> Finally, the final ester product can be obtained by oxidative dehydrogenation of the hemiacetal intermediate, and the metal active sites are regenerated as oxygen reacts with hydrogen on the metal NP surface.

**Scheme 3. Proposed Reaction Pathway**

Irradiation also enhances the surface charge heterogeneity of the alloy NPs, which means that interactions between the alloy NPs and reactant molecules are enhanced.<sup>9</sup> There is a much higher probability that the reactant molecules are adsorbed on the Pd sites on the alloy NPs surface, and Pd sites have a better ability to attract hydrogen, which can promote the hydrogen abstraction steps (both III and V). Overall, the light-excited electrons may facilitate the hydrogen-abstraction steps, which could assist the direct oxidative esterification when the alcohol molecules are adsorbed on the surface of metal NPs.

**4. CONCLUSIONS**

In summary, a stable and reusable catalyst of Au–Pd alloy NPs supported on phosphate anion modified hydrotalcite has been found to be active and selective for the direct oxidative esterification of aliphatic alcohols under visible-light irradiation using molecular oxygen as a benign oxidant. The novel catalyst can be prepared readily by utilizing the “memory effect” of hydrotalcite, followed by the impregnation–reduction of gold and palladium salts to form Au–Pd alloy NPs on the surface of phosphate anion modified hydrotalcite. The catalyst exhibits superior performance for the synthesis of a variety of esters with aliphatic alcohols when irradiated with visible light, achieving good yields without any additives. It is also applicable for oxidative esterification of aryl alcohols and oxidation of secondary aliphatic alcohols to ketones. These catalytic processes are due to the interaction of light-excited electrons from the metal NPs reacting with the substrate molecules, and in these reactions, elevated reaction temperatures and high pressures are not required. The oxidative esterification of aliphatic alcohols involves selective conversion of aliphatic alcohols to the corresponding aldehydes and subsequent esterification of the aldehydes with unreacted alcohol. The reaction rate depends on the number and the energy level of light-excited electrons, which can be tuned by the incident light intensity and wavelength. The base-free catalytic process is simple, cost-effective, and environmentally benign.

**ASSOCIATED CONTENT****Supporting Information**

Supplementary Tables S1–S4, Figures S1–S3, and Scheme S1. This material is available free of charge via the Internet at <http://pubs.acs.org>.

**AUTHOR INFORMATION****Corresponding Author**

hy.zhu@qut.edu.au

**Notes**

The authors declare no competing financial interest.

**ACKNOWLEDGMENTS**

We gratefully acknowledge financial support from the Australian Research Council (ARC DP110104990), Institute of Coal Chemistry, Chinese Academy of Sciences for TPD measurement, supported by the Foundation of State Key Laboratory of Coal Conversion (Grant No. J14-15-605).

**REFERENCES**

- (1) Larock, R. C. *Comprehensive Organic Transformations*; VCH: New York, 1989; p 966 and references therein.
- (2) March, J. *Advanced Organic Chemistry*; Wiley, New York, 1985.
- (3) Lloyd, W. G. *J. Org. Chem.* **1967**, *32*, 2816–2819.
- (4) Larock, R. C. *Comprehensive Organic Transformations: A Guide to Functional Group Preparations*, 2nd ed.; Wiley-VCH, New York, 1999.
- (5) Xu, B.; Liu, X.; Haubrich, J.; Madix, R. J.; Friend, C. M. *Angew. Chem. Int. Ed.* **2009**, *48*, 4206–4209.
- (6) Oliveira, R. L.; Kiyohara, P. K.; Rossi, L. M. *Green Chem.* **2009**, *11*, 1366–1370.
- (7) Miyamura, H.; Yasukawa, T.; Kobayashi, S. *Green Chem.* **2010**, *12*, 776–778.
- (8) Zweifel, T.; Naubron, J. V.; Grutzmacher, H. *Angew. Chem., Int. Ed.* **2009**, *48*, 559–563.
- (9) Arita, S.; Koike, T.; Kayaki, Y.; Ikariya, T. *Chem.—Asian J.* **2008**, *3*, 1479–1485.
- (10) Lu, T.; Du, Z.; Liu, J.; Ma, H.; Xu, J. *Green Chem.* **2013**, *15*, 2215–2221.
- (11) Liu, X.; Wu, J.; Shang, Z. *Synth. Commun.* **2012**, *42*, 75–83.
- (12) Mori, N.; Togo, H. *Tetrahedron* **2005**, *61*, 5915–5925.
- (13) Barluenga, J.; González-Bobes, F.; Murguía, M. C.; Ananthoju, S. R.; González, J. M. *Chem.—Eur. J.* **2004**, *10*, 4206–4213.
- (14) Do, Y.; Ko, S.-B.; Hwang, I.-C.; Lee, K.-E.; Lee, S. W.; Park, J. *Organometallics* **2009**, *28*, 4624–4627.
- (15) Izumi, A.; Obora, Y.; Sakaguchi, S.; Ishii, Y. *Tetrahedron Lett.* **2006**, *47*, 9199–9201.
- (16) Liu, C.; Tang, S.; A. Lei, W. *Chem. Commun.* **2013**, *49*, 1324–1326.
- (17) Esteruelas, M. A.; García-Obregón, T.; Herrero, J.; Oliván, M. *Organometallics* **2011**, *30*, 6402–6407.
- (18) Gowrisankar, S.; Neumann, H.; Beller, M. *Angew. Chem., Int. Ed.* **2011**, *50*, 5139–5143.
- (19) Schleker, P. P. M.; Honeker, R.; Klankermayer, J.; Leitner, W. *ChemCatChem* **2013**, *5*, 1762–1764.
- (20) Shahane, S.; Fischmeister, C.; Bruneau, C. *Catal. Sci. Technol.* **2012**, *2*, 1425–1428.
- (21) Nielsen, M.; Junge, H.; Kammer, A.; Beller, M. *Angew. Chem., Int. Ed.* **2012**, *51*, 5711–5713.
- (22) Meijer, R. H.; Ligthart, G. B. W. L.; Meuldijk, J.; Vekemans, J. A. J. M.; Hulshof, L. A.; Mills, A. M.; Kooijman, H.; Spek, A. L. *Tetrahedron* **2004**, *60*, 1065–1072.
- (23) Van Doorslaer, C.; Schellekens, Y.; Mertens, P.; Binnemans, K.; De Vos, D. *Phys. Chem. Chem. Phys.* **2010**, *12*, 1741–1749.
- (24) Jagadeesh, R. V.; Junge, H.; Pohl, M.-M.; Radnik, J.; Brückner, A.; Beller, M. *J. Am. Chem. Soc.* **2013**, *135*, 10776–10782.
- (25) Powell, A. B.; Stahl, S. S. *Org. Lett.* **2013**, *15*, 5072–5075.
- (26) Sarina, S.; Zhu, H.; Jaatinen, E.; Xiao, Q.; Liu, H.; Jia, J.; Chen, C.; Zhao, J. *J. Am. Chem. Soc.* **2013**, *135*, 5793–5801.
- (27) Bezen, M. C. I.; Breitkopf, C.; Lercher, J. A. *ACS Catal.* **2011**, *1*, 1384–1393.
- (28) Orthman, J.; Zhu, H. Y.; Lu, G. Q. *Sep. Purif. Technol.* **2003**, *31*, 53–59.

- (29) Gupta, N. K.; Nishimura, S.; Takagaki, A.; Ebitani, K. *Green Chem.* **2011**, *13*, 824–827.
- (30) Noujima, A.; Mitsudome, T.; Mizugaki, T.; Jitsukawa, K.; Kaneda, K. *Angew. Chem., Int. Ed.* **2011**, *50*, 2986–2989.
- (31) Debecker, D. P.; Gaigneaux, E. M.; Busca, G. *Chem.—Eur. J.* **2009**, *15*, 3920–3935.
- (32) Prodan, E.; Radloff, C.; Halas, N. J.; Norlander, P. *Science* **2003**, *302*, 419–422.
- (33) Sarina, S.; Zhu, H. Y.; Xiao, Q.; Jaatinen, E.; Jia, J.; Huang, Y.; Zheng, Z.; Wu, H. *Angew. Chem., Int. Ed.* **2014**, *53*, 2935–2940.
- (34) Long, R.; Mao, K.; Gong, M.; Zhou, S.; Hu, J.; Zhi, M.; You, Y.; Bai, S.; Jiang, J.; Zhang, Q.; Wu, X.; Xiong, Y. *Angew. Chem., Int. Ed.* **2014**, *53*, 3205–3209.
- (35) Penner, S.; Bera, P.; Pedersen, S.; Ngo, L. T.; Harris, J. J. W.; Campbell, C. T. *J. Phys. Chem. B* **2006**, *110*, 24577–24584.
- (36) Zhang, Y.; Yang, Z.; Wu, M. *Phys. Chem. Chem. Phys.* **2014**, *16*, 20532–20536.
- (37) Su, F. Z.; Ni, J.; Sun, H.; Cao, Y.; He, H. Y.; Fan, K. N. *Chem.—Eur. J.* **2008**, *14*, 7131–7135.
- (38) Sarina, S.; Waclawik, E. R.; Zhu, H. Y. *Green Chem.* **2013**, *15*, 1814–1833.
- (39) Xiao, Q.; Jaatinen, E.; Zhu, H. Y. *Chem.—Asian J.* **2014**, *9*, 3046–3064.
- (40) Kale, M. J.; Avanesian, T.; Christopher, P. *ACS Catal.* **2014**, *4*, 116–128.
- (41) Kowalska, E.; Abea, R.; Ohtania, B. *Chem. Commun.* **2009**, *2*, 241–243.
- (42) Tanaka, A.; Sakaguchi, S.; Hashimoto, K.; Kominami, H. *ACS Catal.* **2013**, *3*, 79–85.
- (43) Xiao, Q.; Sarina, S.; Bo, A.; Jia, J.; Liu, H.; Arnold, D. P.; Huang, Y.; Wu, H.; Zhu, H. Y. *ACS Catal.* **2014**, *4*, 1725–1734.
- (44) Avanesian, T.; Christopher, P. *J. Phys. Chem. C* **2014**, *118*, 28017–28031.
- (45) Kale, M. J.; Avanesian, T.; Xin, H.; Yan, J.; Christopher, P. *Nano Lett.* **2014**, *14*, 5405–5412.
- (46) Christopher, P.; Xin, H. L.; Linic, S. *Nat. Chem.* **2011**, *3*, 467–472.
- (47) Linic, S.; Christopher, P.; Ingram, D. B. *Nat. Mater.* **2011**, *10*, 911–921.
- (48) Christopher, P.; Xin, H. L.; Marimuthu, A.; Linic, S. *Nat. Mater.* **2012**, *11*, 1044–1050.
- (49) Olsen, T.; Gavnholt, J.; Schiøtz, J. *Phys. Rev. B* **2009**, *79*, 035403.
- (50) Bonn, M.; Funk, S.; Hess, C.; Denzler, D. N.; Stampf, C.; Scheffler, M.; Wolf, M.; Ertl, G. *Science* **1999**, *285*, 1042–1045.
- (51) Wang, F.; Li, C.; Chen, H.; Jiang, R.; Sun, L. D.; Li, Q.; Wang, J.; Yu, J. C.; Yan, C. H. *J. Am. Chem. Soc.* **2013**, *135*, 5588–5601.
- (52) Zope, B. N.; Hibbitts, D. D.; Neurock, M.; Davis, R. J. *Science* **2010**, *330*, 74–78.